6-1-1970

The effect of precipitation of non-magnetic inclusions on the coercive field and the initial permeability of alpha-iron.

Mohammad Saduddin Khan
University of Windsor

THE EFFECT OF PRECIPITATION OF NON-MAGNETIC INCLUSIONS ON THE COERCIVE FIELD AND THE INITIAL PERMEABILITY OF α-IRON

by

MOHAMMAD SADUDDIN KHAN

A THESIS

SUBMITTED TO THE FACULTY OF GRADUATE STUDIES

THROUGH THE DEPARTMENT OF ELECTRICAL ENGINEERING

IN PARTIAL FULFILLMENT OF THE

REQUIREMENTS FOR THE DEGREE OF

MASTER OF APPLIED SCIENCE

University of Windsor

June, 1970

AIBr0477

APPROVED BY

307765

ABSTRACT

Experimental investigations have been carried out to determine the effects of non-magnetic inclusions on the technically important magnetic properties, the coercive field and the initial permeability of α-iron. An attempt has been made to derive a quantitative relation between the magnetic properties and structural defects.

The results are discussed in the light of the theory of ferromagnetic hysteresis.

ACKNOWLEDGEMENT

The author wishes to express his sincere thanks to Dr. A.H. Qureshi for the continuous guidance and encouragement accorded to him at all stages of this work. Financial assistance provided by N.R.C. is greatly appreciated.

TABLE OF CONTENTS

LIST OF TABLES

LIST OF FIGURES

CHAPTER I

INTRODUCTION

In the study of ferro-magnetic hysteresis, the coercive field and the initial permeability of the materials have great importance. Many theories have been developed in an attempt to understand these properties quantitatively and to relate them to the microscopic structure of the material. It is a well known fact that these properties are associated with the Bloch wall movement.

The fundamental phenomena of magnetization, i.e. the Bloch wall movement and the rotation of the spin direction etc., are strongly affected by lattice disturbances such as stresses, impurities and inclusions in these materials.

In the present work, inclusions were introduced in α-Fe by precipitation and coagulation of copper in super-saturated Fe-Cu alloys.

The behavior of the coercive field and the initial permeability of the material have been studied in the presence of such inclusions.

The first portion of this work deals with the theory of ferromagnetic hysteresis, the nature of the coercive field and the initial permeability of the materials, and the effect of the distribution, shape and size of the inclusions on these properties.

CHAPTER II

THEORY AND LITERATURE REVIEW

The atomic origins of magnetism are generally understood to be the orbital motion and the spin of electrons.

Materials have various magnetic properties due to their different electronic configurations and they can be classified under the following headings:

(i) Diamagnetism

(ii) Paramagnetism

(iii) Ferromagnetism, antiferromagnetism, ferrimagnetism.

All of these phenomena are discussed extensively in literature. Due to its importance to this work, the ferromagnetic phenomenon will be further discussed.

THE PHENOMENON OF FERROMAGNETISM:

Ferromagnetism results from a strong interaction of spin alignment in various magnetic domains separated by domain walls in the absence of an external magnetizing field and each domain is spontaneously magnetized in an easy direction of magnetization of the crystal structure.

The domains are so arranged that the net effect of spontaneous magnetization of the whole piece of material is zero. The spin arrangement is disturbed by increasing temperature due to thermal agitation; therefore, the saturation magnetization is temperature dependent. Above the Curie point, the susceptibility of the magnetic material obeys the Curie-Weiss

Law. The presence of saturation magnetization and hysteresis are important features in ferromagnetism.

THEORY OF FERROMAGNETISM: (1),(2)

2.1 Quantum Theory:

Ferromagnetism is the result of an ordered alignment of atomic magnetic moments, and there are two possible origins of the atomic magnetic moments. One is the orbital motion of the electron and the other is the spin of the electron. A simple model of an atom contains an electron moving around its nucleus with an angular velocity ω . Due to the motion of this electron which makes $\frac{\omega}{2\pi}$ revolutions per second, a current $-\frac{e\omega}{2\pi}$ (ampere) is produced where -e is the electronic charge. The magnetic moment due to this current may be written as:

$$M = -\mu_o \frac{e\omega}{2\pi}(\pi r_e^2) = -\tfrac{1}{2}\mu_o e\omega r_e^2 \qquad (2.1.1)$$

when r_e is the radius of the orbit in which the electron is moving and μ_o is the permeability of the vacuum. The angular momentum of the circular motion is:

$$P = m\omega r_e^2 \qquad (2.1.2)$$

where m is the mass of an electron.

Using (2.1.2) in (2.1.1)

$$M = -\frac{\mu_o eP}{2m} \qquad (2.1.3)$$

According to the quantum theory, an electron can move in any orbit where it satisfies the relation

$$P = n\hbar \qquad (2.1.4)$$

where $\hbar = \frac{h}{2\pi}$ and h is the Planck constant, n is an integer, 1,2,.....

Using (2.1.4) in (2.1.3)

$$M = -\frac{n \mu_o \hbar e}{2m} \qquad (2.1.5)$$

or

$$M = -nM_B \qquad (2.1.6)$$

where $M_B = \frac{\mu_o \hbar e}{2m}$, called the Bohr magneton.

Thus, according to (2.1.6), the magnetic moment of the orbital motion can change its value by integral multiples of M_B units.

In the case of angular moment for spin motion;

$$M = -\frac{\mu_o e P}{m} \qquad (2.1.7)$$

because the electron spins around its own axis with an angular momentum $\pm \frac{\hbar}{2}$. The most general relation for magnetic moment may be written as

$$M = -\frac{eg \mu_o}{2m} P \qquad (2.1.8)$$

will give the magnetic moment for orbital motion when g=1 and for spin motion when g=2.

The factor "g" is called the "gyromagntic ratio". The value of "g" could be found by two methods: (1) gyromagnetic experiment; (2) ferromagnetic resonance. Hence, one could find which mechanism is responsible for ferromagnetism in a material.

The magnetic moment of a free atom which contains many electrons is given:

$$M = -g M_B J \qquad (2.1.9)$$

where J is the resultant total angular momentum, due to spin-orbit interaction. J can have values 0, ½, 1, $\frac{3}{2}$, ...

From quantum mechanical treatment,

$$g = 1 + \frac{J(J+1) + S(S+1) - L(L+1)}{2J(J+1)} \qquad (2.1.10)$$

where $\overrightarrow{S}$ is the resultant spin-vector

$\overrightarrow{L}$ is the resultant orbital-vector.

When $L = 0$ $J = S$

i.e. J is only due to spin motion.

$\therefore g = 2$

When $S = 0$ $J = L$

i.e. J is only due to orbital motion

$\therefore g = 1$

In ferromagnetic materials, g has approximately the value of 2. Hence the ferromagnetic phenomenon is due to spin motion of the electrons and not to their orbital motion. Therefore, any change of magnetization in a ferromagnetic material will change only the electrons' spin directions and not their orbits. The orbits of the electrons are also slightly orientated because the "g" measured for iron is approximately 1.94, cobalt 1.85, nickel 1.90 from the gyromagnetic effect experiment.

Generally the contribution of the orbital magnetic moment which is almost quenched by the crystalline field produced by the surrounding atoms in ferromagnetic materials, may

not be quenched in the free atoms of some ferromagnetic materials such as rare earth metals. Therefore ferromagnetism will be due to both spin and orbital magnetic moments.

2.2. WEISS THEORY OF FERROMAGNETISM (2),(3),(4)

This theory has been derived, to some extent, from the Langevin theory of paramagnetism, which states that each atom or molecule has a magnetic moment which aligns itself parallel to the direction of the applied field. Thermal agitation opposes this alignment of magnetic moments. According to the Langevin theory, a field of the order 10^6 Oe will be required to cause saturation magnetization in ferromagnetic materials, while in practice the maximum field is of the order 10^3 Oe.

This contradiction was explained by Weiss who stated that in ferromagnetic materials there is an intermolecular field which is proportional to the degree of magnetization.

∴ the total field inside the material is

$$H_t = H_a + NI \qquad (2.2.1)$$

I = intensity of magnetization

H_a = applied field

N = molecular field constant

According to the Langevin theory of paramagnetism, a relation between the intensity of magnetization of a paramagnetic substance and the applied field H_a is given by:

$$I = I_s B_J(\alpha) \qquad (2.2.2)$$

where the Brillouin function

$$B_J(\alpha) = \frac{2J+1}{2J} \coth \frac{2J+1}{2J}\alpha - \frac{1}{2J} \coth \frac{\alpha}{2J}$$

$$\alpha = \frac{MH_a}{kT} = \frac{gM_B JH_a}{kT} \qquad (2.2.2a)$$

and k is Boltzmann's constant.

When $J = \frac{1}{2}$, i.e. for the spin dipole moment of a single uncompensated electron, the Brillouin function reduces to

$$B_{J=\frac{1}{2}}(\alpha) = \tanh(\alpha) \qquad (2.2.3)$$

For ferromagnetic material one can write (2.2.2) as,

$$\frac{I}{I_s} = \tanh(\alpha) \qquad (2.2.4)$$

where

$$\alpha = \frac{M(H_a+NI)}{kT} \qquad (2.2.2a)$$

The molecular field in the case of ferromagnetic materials is much greater than any applied field:

when $H_a = 0$ and $\Theta = \frac{MNI_s}{k}$

$$\frac{I_{spon}}{I_s} = \tanh \frac{I_{spon}/I_s}{T/\Theta} \qquad (2.2.5)$$

where I_{spon} is the spontaneous magnetization due to the molecular field.

(2.2.5) shows that below the Curie temperature, the intensity of magnetization has a definite value even for $H_a=0$. Theoretical values from (2.2.5) and experimental values show a fair agreement (Fig.2.2.1).

Ferromagnetism above the Curie Temperature:

All ferromagnetic materials exhibit paramagnetism above the Curie temperature Θ : as I_s falls to zero at temperature Θ, the internal field also falls to zero.

The application of an external field above the Curie temperature Θ results in a small paramagnetic induction; and the exchange interaction's contribution to an internal molecular field NI will not be large as compared to H_a as in the case below the Curie temperature. The first term of the Brillouin function in the series expansion will be sufficient in (2.2.2) and, using (2.2.2a) we get -

$$\frac{I}{I_s} = \frac{J+1}{3J} \quad \alpha = \frac{(J+1)gM_B(H_a+NI)}{3kT} \qquad (2.2.6)$$

For a volume susceptibility χ we can write:

$$\chi = \frac{I}{H_a} = \frac{C}{T-\Theta} \qquad (2.2.7)$$

where $C = \frac{I_s g M_B (J+1)}{3k}$

and $\Theta = NC$.

The Curie Weiss Law (2.2.7) shows a straight line when $\frac{1}{\chi}$ is expressed as a function of temperature with an intercept at temperature Θ , where Θ is the Curie temperature.

The observed behavior for iron, nickel and cobalt is shown in Figure (2.2.2). There is good agreement between the theory and the observed values except near the Curie point.

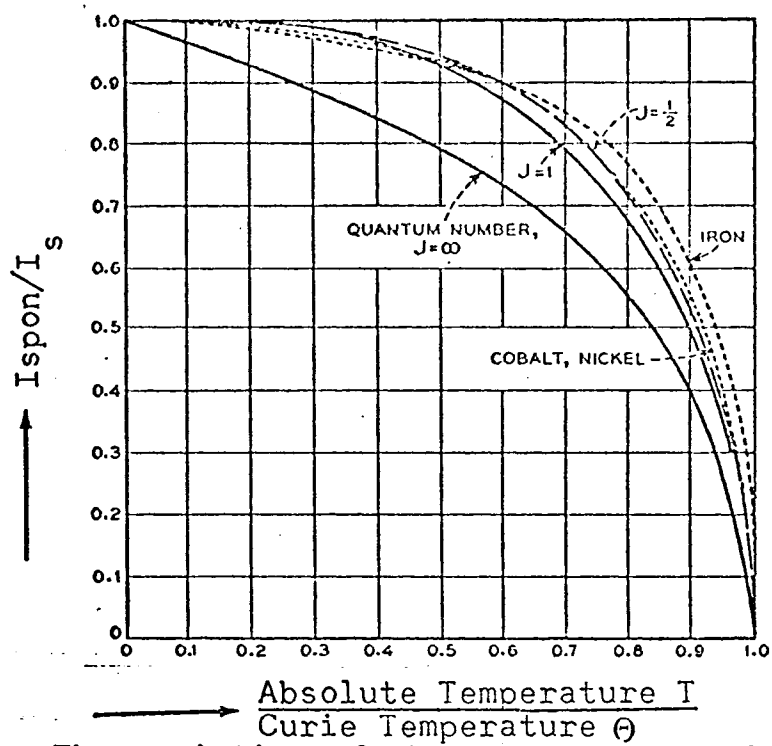

Fig.2.2.1 - The variation of the reduced magnetizations of iron, cobalt and nickel with reduced temperature.

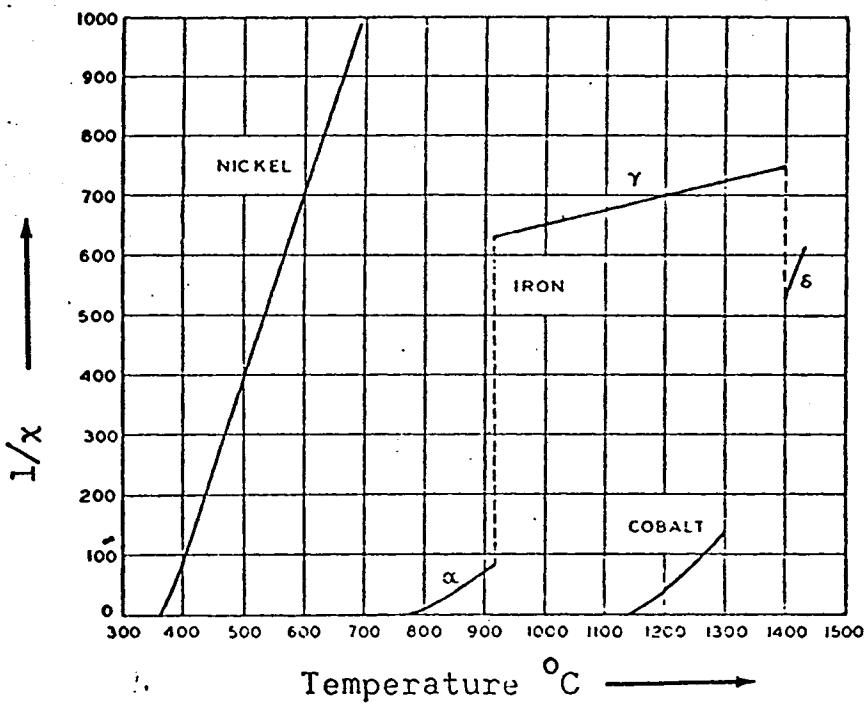

Fig.2.2.2 - The variation of the reciprocal of volume susceptibility of iron, cobalt and nickel with temperature.

2.3 DOMAIN THEORY:

The objection to both the quantum theory and the Weiss field theory is that the ferromagnetic material must show magnetism without an applied external field. This objection is not valid, since these materials could exist in the unmagnetized state. The problem is solved by the Domain theory which states that a ferromagnetic material contains many small magnetic domains, called Weiss' regions and these domains are so arranged in the ferromagnetic material that the net effect of the magnetic moment of the entire piece is zero in the absence of an external field. Each domain by itself is spontaneously magnetized in the direction of the preferred magnetization of the crystal when an external field is applied, the domains, having spontaneous magnetization in the direction of the applied field, are enlarged at the expense of the others so that a resultant magnetic moment is obtained.

The domain size varies for different materials depending on the impurities present and their physical nature. Each domain contains all of the spins aligned in a particular easy direction of magnetization of the material to minimize anisotropy energy, and is separated by boundaries called Bloch walls.

Domain walls can be further classified as 180^{o} walls, in which the spins rotate 180^{o} from one domain to the other, and as 90^{o} walls, in which the spins rotate approximately 90^{o} as shown in figure (2.3.1).

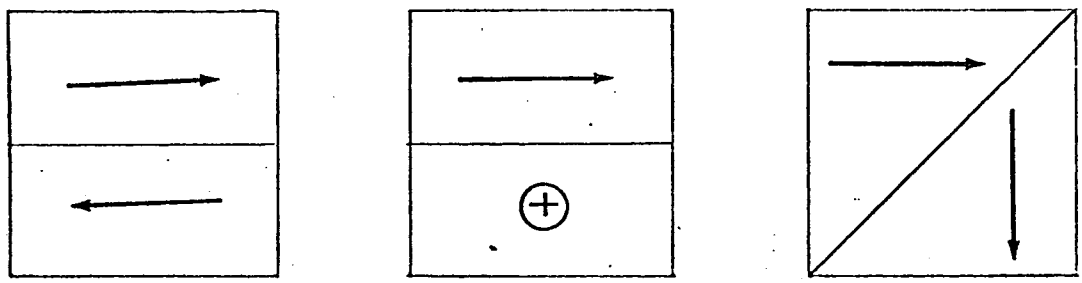

Fig.2.3.1 - Different kinds of magnetic domain boundaries.

The domain walls could be shifted by applying an external field. The application of weak fields shifts the domain boundaries temporarily, i.e., the boundaries regain their original position on removal of the applied field. However, the application of strong fields permanently shifts the domain walls from their original positions. Still stronger fields cause these domains to rotate and align themselves in the direction of the field.

Figure (2.3.2) shows the effect of external fields on the magnetization of a magnetic material in the three stages described above in the areas marked I, II and III. The process of magnetization in the initial stages occurs in steps called Barkhausen jumps, where the domain walls move under the influence of the applied field. However, these jumps in a multiple domain material are such that the resulting curve appears to be continuous. The presence of impurities or stresses etc. in ferromagnetic materials strongly affect the movement of the Bloch wall. The coercive field and the initial permeability, which are properties of technical interest, are associated with the Bloch wall movement and hence are affected by impurities, inclusions or stresses present in ferromagnetic materials. This will be discussed in detail in the following text.

2.4 GENERAL THEORIES OF THE INITIAL PERMEABILITY AND THE COERCIVE FIELD: (1)

It is understood that the initial permeability is related to the reversible movement of the domain walls, and the coercive field is related to the irreversible movement of the domain walls for any ferromagnetic material.

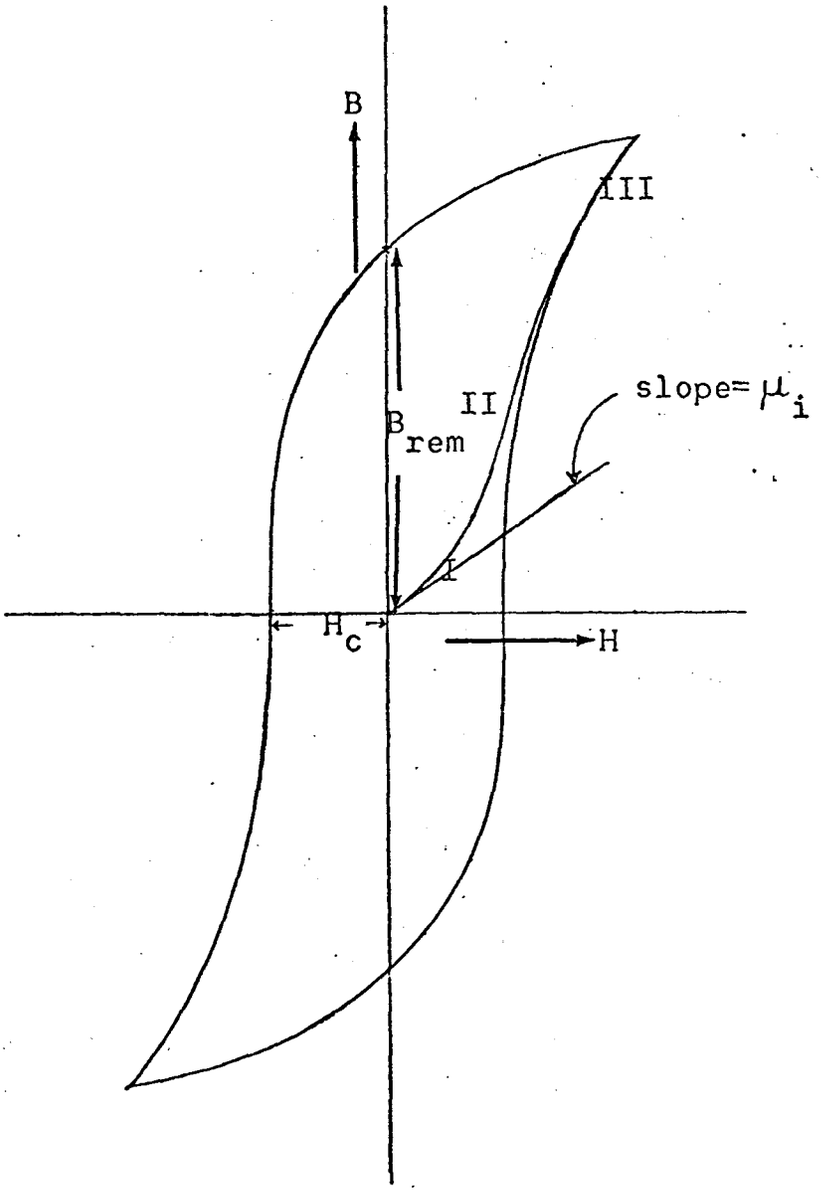

Fig.2.3.2 - Hysteresis loop.

2.4 (a) Reversible magnetic domain wall displacement and the initial permeability:

Consider that a plane domain wall is displaced in non-uniform material and the energy of the wall per unit area is E_w. E_w changes with the wall displacement along x as in figure (2.4.1).

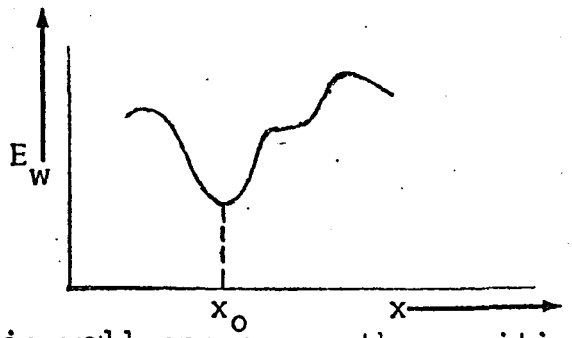

Fig.2.4.1 - Domain wall energy vs the position of the wall.

When no external field is applied, the wall stays at some minimum pt. x_o in figure (2.4.1), where the energy gradient is zero.

i.e. $$\frac{\partial E_w}{\partial x} = 0 \qquad (2.4.1)$$

The energy of the wall near the stable point in the first approximation is:

$$E_w = \tfrac{1}{2} \alpha x^2 \qquad (2.4.2)$$

where α is curvature of potential valley.

The energy supplied by the external magnetic field H in a direction which makes an angle Φ with I_s, as in figure (2.4.2), may be written as:

$$E_H = -2 I_s H(cs\Phi)x \qquad (2.4.3)$$

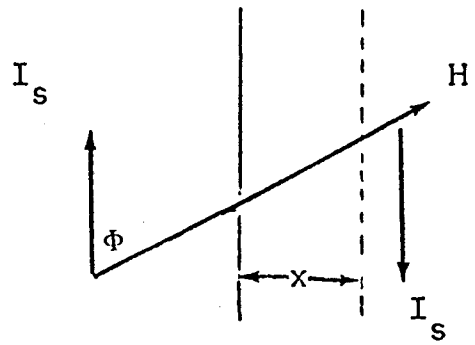

Fig.2.4.2 - Displacement of a 180° wall.

When a 180° wall is displaced by x, the result is a change in the magnetization of the wall as $2I_s x$, per unit area of the wall. The domain wall always keeps its total energy to a minimum.

$$\frac{\partial E_t}{\partial x} = \frac{\partial (E_w + E_H)}{\partial x} = 0 \qquad (2.4.4)$$

$$\frac{\partial (\frac{1}{2}\alpha x^2 - 2I_s H(\cos\Phi)x)}{\partial x} = 0$$

$$\alpha x - 2I_s H \cos\Phi = 0$$

$$x = \frac{2I_s \cos\Phi H}{\alpha} \qquad (2.4.5)$$

The magnetization in the direction of the field increases by $2I_s (\cos\Phi)x$, due to wall displacement so that the total magnetization of the wall per unit volume is given by

$$I = \frac{4I_s^2 \cos_\Phi^2}{\alpha} SH \qquad (2.4.6)$$

where S is the total area of the 180° wall per unit volume.

the initial susceptibility is:

$$\chi_i = \frac{I}{H} = \frac{4I_s^2 \cos\Phi^2 S}{\alpha} \qquad (2.4.7)$$

For a cubic structure such as iron, for a positive anisotropy constant K_1, the average of cosine^2 of the angles between the directions of the various dipoles and that of the applied magnetic field H is equal to 1/3.

$$\chi_{i_{180^\circ}} = \frac{4I_s^2 S}{3\alpha} \qquad (2.4.8)$$

The initial permeability could be calculated by

$$\mu_i = 1+\chi_i \qquad (2.4.9)$$

Kondorsky [5] proposed that the origin of internal stress was responsible for the fluctuation of wall energy. Kersten [6] developed the relation for χ_i by assuming the sinusoidal variation of internal stress.

$$\sigma = \sigma_o \cos 2\pi \frac{x}{\ell} \qquad (2.4.10)$$

where ℓ is the wavelength of the spatial variation of internal stress. For $K = K_1 - \frac{3}{2}\lambda\sigma_o \cos 2\pi \frac{x}{\ell}$ and $\gamma = 2\sqrt{A\left(K_1 - \frac{3}{2}\lambda\sigma_o \cos 2\pi \left(\frac{x}{\ell}\right)\right)}$, the values of α and S for (2.4.8) may be written as:

$$\alpha = \frac{2\pi^2 \lambda \sigma_o \delta}{\ell} \qquad (2.4.11)$$

$$S = \frac{3}{\ell} \qquad (2.4.12)$$

assuming that the internal stress fluctuates in x,y,z directions, where δ is the Bloch wall thickness.

γ = surface energy of the wall; λ = magnetostriction constant; A = exchange energy constant.

$\therefore$ (2.4.8) could be written [1]

$$\chi_{i_{180^o}} = \frac{2I_s^2}{\pi^2 \lambda \sigma_o} \frac{\ell}{\delta} \qquad (2.4.13)$$

In (2.4.13), the initial susceptibility decreases with a decrease of ℓ . For $\ell < \delta$ (2.4.13) is not valid and for $\ell \simeq \delta$, the initial susceptibility takes the minimum value:

$$\chi_{i_{180^o}} = \frac{2I_s^2}{\pi^2 \lambda \sigma_o} \qquad (2.4.14)$$

(2.4.13) gives nearly the same value, if susceptibility is considered due to rotation magnetization caused by stress,

$$\chi_{i_{rot}} = 2I_s^2/9\lambda\sigma \qquad (2.4.15)$$

In a similar way, one can calculate the initial susceptibility due to reversible displacement of the 90° wall [1].

as $$\chi_{i_{90^o}} = \frac{2I_s^2}{3\alpha} S \qquad (2.4.16)$$

for the equal distribution of 90^o walls over four possible orientations, i.e. $<110>$.

Considering the stress of the sinusoidal nature, the values of α and S for (2.4.16) is [1]

$$\alpha = \frac{3\pi\lambda_{100}\sigma}{\ell} \qquad (2.4.17)$$

$$S = \frac{6}{\ell} \qquad (2.4.18)$$

assuming that internal tension changes in all $[110]$ directions. λ_{100} is the saturation magnetostriction; . . (2.4.16) may be written:

$$\chi_{i_{90^o}} = \frac{4I_s^2}{3\pi\lambda_{100}\sigma} \qquad (2.4.19)$$

For negative K_1

$$\chi_{i_{90^o}} = \frac{2I_s^2}{3\pi\lambda_{111}\sigma} \qquad (2.4.20)$$

The relations (2.4.19) and (2.4.20) give nearly the same value for $\chi_i 90^o$. The theoretical values calculated for iron and the measured values are in fair agreement [1].

(b) Reversible domain wall displacement (in the presence of nonmagnetic inclusions) and the initial permeability:

For the first time Kersten [6] considered the reversible wall displacement in the presence of the nonmagnetic inclusions in which he postulated that the domain wall sticks to the nonmagnetic inclusions and thus the wall area and the

wall energy are reduced. When an external field is applied, the wall is displaced and its area and energy are increased. He calculated the initial permeability and the coercive field in this theory.

Due to Neel's[7] theory of free poles and internal strain which are responsible for the restoring force on the Bloch wall, Kersten[8] modified his previous assumptions and calculated the initial permeability by the assumption of the flexibility of domain walls.

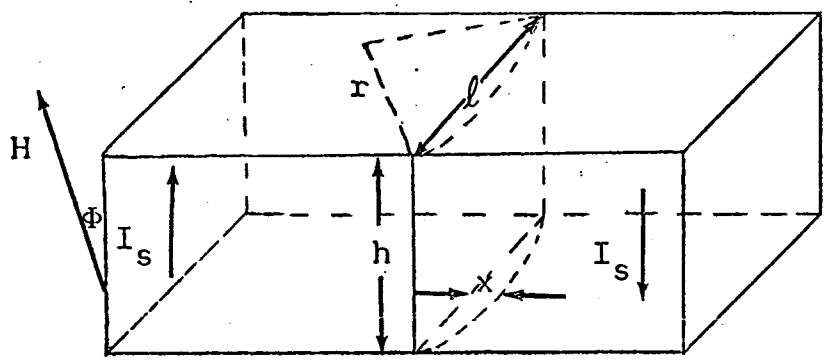

Fig.2.4.3 - An expanded 180° wall under the action of a magnetic field.

Consider that the 180° wall is fixed at both ends as in figure (2.4.3). Let the application of a field H be in the direction Φ as in the figure and the area S of the wall be displaced through distance x.

Then the work done by the field is given by:

$$W = -2I_s H(cs\Phi)Sx \qquad \text{(2.4.21)}$$

$\therefore$ Pressure exerted on the wall:

$$P = -\frac{1}{S}\frac{\partial W}{\partial x} = 2I_s Hcs\Phi \qquad \text{(2.4.22)}$$

Due to this pressure, the wall is bent in a cylindrical shape as shown in figure (2.4.3). The radius of curvature

of the wall could be related to H as:

$$\frac{\gamma}{r} = 2I_s H \cos\Phi \qquad (2.4.23)$$

where γ is the surface energy of the wall.

The change in volume of the positive magnetization domain.

$$\Delta v = 2/3\, \ell\, h x \qquad (2.4.24)$$

where h and ℓ are shown in figure (2.4.3).

$\therefore$ the increase in magnetization is

$$I = 4/3\ I_s(\cos\Phi)Sx \qquad (2.4.25)$$

Using the geometrical relation:

$$x = \frac{\ell^2}{8r} \qquad (2.4.26)$$

Substituting x in (2.4.25) from (2.4.26), and using (2.4.23), the relation (2.4.25) may be written as

$$I = \frac{S\ell^2 I_s^2}{3\gamma}(\cos^2\Phi)H \qquad (2.4.27)$$

For all easy directions, $\overline{\cos^2\Phi} = 1/3$, the susceptibility is calculated as $(\chi_i = I/H)$,

$$\chi_{i180^\circ} = \frac{S_{180^\circ}\, \ell^2\, I_s^2}{9\gamma_{180^\circ}} \qquad (2.4.28)$$

Similarly $\chi_{i90^\circ} = \dfrac{S_{90^\circ}\, \ell^2\, I_s^2}{18\, \gamma_{90^\circ}}$ (2.4.29)

If it is assumed that the inclusions are distributed at the corners of a simple cubic lattice with lattice constant ℓ, then the total area of the 180° wall may be written as[1]:

$$S = \frac{2}{\ell}; \quad \therefore \chi_i = \frac{2I_s^2\,\ell}{9\gamma} \qquad (2.4.30)$$

In the case of iron, the permeability could be explained by this mechanism.

(c) Irreversible magnetic domain wall displacement and the coercive field.

Consider a plane Bloch wall which moves to the right and its energy changes as in figure (2.4.4).

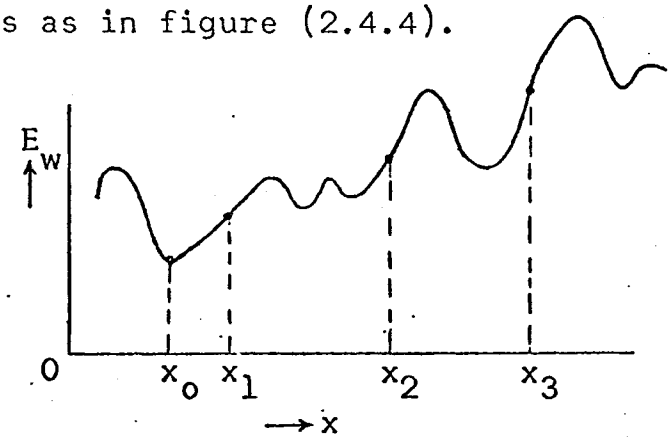

Fig.2.4.4 - Variation of the wall energy as a function of the displacement of the wall.

The application of an external field H will exert a pressure P as in (2.4.22), i.e., $P = 2 I_s H \cos\Phi$

The wall will be displaced from position x_0 to x_1,

where $\frac{\partial E_w}{\partial x} = P = 2 I_s H \cos\Phi$ _____(2.4.31).

If the maximum gradient of the wall energy is at x_1, a further increase of the field will result in an irreversible displacement of the wall, taking the wall to x_2 or x_3.

Therefore the critical value of H, where the wall would take an irreversible displacement, can be given:

$$H_o = \frac{1}{2 I_s \cos\Phi} \left(\frac{\partial E_w}{\partial x}\right)_{max} \quad \text{_____(2.4.32).}$$

If the initial internal stress is sinusoidal in nature as (2.4.10), then,

$$\left(\frac{\partial \gamma}{\partial x}\right)_{max} = \frac{2\pi\lambda\sigma_o\delta}{\ell} \quad \text{_____(2.4.33)}$$

where δ is the Bloch wall thickness. Since the Bloch wall does not change in area,

$\therefore$ $E_w = \gamma$, (2.4.32) becomes

$$H_o = \frac{\pi \lambda \sigma_o}{I_s \cos \Phi} \frac{\delta}{\ell} \qquad (2.4.34)$$

The maximum value of H_o is found for $\delta = \ell$

$$H_c = (H_o)_{max} = \frac{\pi \lambda \sigma_o}{I_s \cos \Phi} \qquad (2.4.35)$$

The value of the coercive field obtained from (2.4.35) agrees favourably with values obtained for various materials after they were being deformed[1].

(d) Irreversible magnetic domain wall displacement and the coercive field: (Foreign body theory).

Assume that the wall is fixed at two ends and could be expanded by the application of an external field as in figure (2.4.5).

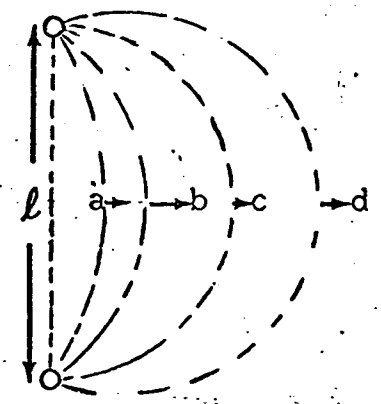

Fig.2.4.5 - Reversible and irreversible expansion of a wall.

The radius of the curvature of the wall is given by (2.4.23). In this relation r should decrease as H increases. In figure (2.4.5), curves a,b,and c show the positions of the wall with increasing applied field. For curve c, which is a semi-circle, $r = \frac{\ell}{2}$. Further increase in the applied field causes further

expansion in the wall area so that the radius of curvature starts to increase ($>\ell/2$) and the wall expansion is discontinuous. The critical value of field H_o could be obtained by substituting the minimum value of $r = \frac{\ell}{2}$ in (2.4.23) and we get

$$H_{o180^\circ} = \frac{\gamma}{I_s \ell \cos\Phi} \qquad \text{(2.4.36)}$$

and similarly for a 90° wall:

$$H_{o90^\circ} = \frac{\sqrt{2}\,\gamma}{I_s \ell \cos\Phi} \qquad \text{(2.4.37)}$$

If the binding force at the fixed points is very strong, the coercive field will be determined by the surface tension of the wall, independent of the manner of constraint. If the binding force is not very strong, the wall will leave the fixed points (i.e. non-magnetic inclusions, etc..) before expanding to the shape where $r = \frac{\ell}{2}$, as indicated by the shape c in figure (2.4.6).

Using this model, Kersten [8] explained the coercive field (H_c) of iron-nickel alloy and the temperature dependence of the coercive field (H_c) for iron. In his original paper, he considered dislocations to be fixed points in the development of the above theory.

Dijkstra and Wert[10] have given a theory for the coercive field in the case of spherical non-magnetic inclusions (iron-carbide) in α iron. The coercive field is considered to be due to two effects: (1) the surface tension of the Bloch wall and (2) the internal magnetic poles. The coercive field, according to this theory and their experimental work, depends on both the total volume fraction of inclusions

and the state of dispersion. A rise in the coercive field could be explained by the surface tension effect of the Bloch wall. The maximum of the coercive field is reached when the diameter of the precipitate reaches $d \simeq \delta$, (Bloch wall thickness). The coercive field then begins to decrease because of the creation of internal magnetic poles around the inclusions, thereby producing secondary domains and the surface tension of the Bloch wall being no longer dominant.

The latest experimental results and theory developed for the coercive field are given by Qureshi [11] in the case of non-magnetic inclusions (copper).

The coercive field was found to follow the relation:

$$\log \ln \frac{\Delta(H_c)_{max}}{\Delta(H_c)_{max} - \Delta(H_c)_t} = n \log t - n \log \tau \qquad (2.4.38)$$

$\Delta (H_c)_{max}$ is the maximum increase in H_c at the given annealing temperature;

$\Delta (H_c)_t$ is the rise in coercive field after annealing duration (t) at a given temperature.

n and τ are constants as defined in [13][14][15].

The relation (2.4.38) has been derived from the kinetics of precipitation [13][14][15] under the assumption that $\Delta (H_c)_{max}$ is reached when a non-magnetic phase is precipitated. No theory has been proposed for the initial permeability which has been found to decrease by about 80% of its initial value in its very early stages and then to remain constant.

Although his assumption of the proportionality of $\Delta(H_c)_{max}$ to the total amount of precipitate was violated by his own experimental investigations in that coagulation followed the complete precipitation of the copper in his alloys, the shape of the precipitate particles was found to be the same as expected for (2.4.38). He also measured the size, the distance between any two particles and the number of particles microscopically for various time intervals at different temperatures.

CHAPTER III

EXPERIMENTAL PROCEDURE

Specimens were cut from sheets of 0.022 cm. and 0.032 cm. thickness of Fe-2.02% Cu and Fe-1.56% Cu alloys respectively. The specimens were 120 mm. long and 15 mm. wide. These specimens were annealed at a temperature of 865°C for about 10 hours in a hydrogen atmosphere to bring the copper into perfect solution with iron[12] and to relieve the specimens of any other stresses.

After heat treatment at a temperature of 865°C, these specimens were quenched at the end of the tube furnace and cooled externally by a copper coil through which cold water circulated. It is assumed that the structural state of an alloy, heat treated at any particular temperature, is preserved when quenched in this manner. These specimens were aged at 755°, 775°, 795° and 810°C for various durations and the coercive field and initial permeability measured at various stages of precipitation. The selection of these temperatures was made in order to decrease the time for precipitation and coagulation of the precipitate particles, to achieve the maximum of the coercive field in a minimum period, and to study the behaviour of H_c beyond its maximum. The initial permeability was also measured in

parallel to these investigations. Fe-1.0% Cu, Fe-2.02% Cu, Fe-3.0% Cu alloys were heat treated in hydrogen atmosphere for 6 hours at 900°C and then aged for 12 hours at 700°C to get the supersaturated copper precipitated. The behaviour of the coercive field of these alloys was studied as a function of temperature.

All the observations of the coercive field and the initial permeability of the isothermal heat treatments were made at room temperature. The initial permeability was measured by a ballistic galvanometer. The coercive field was measured using Foster's coercimeter.

CHAPTER IV

RESULTS AND DISCUSSION

The ratio of the coercive field (H_c) at various time intervals during aging to its initial value (H_{c_o}) and the ratio of the initial permeability (μ_i) at various time intervals to its initial value (μ_i)o have been plotted for different temperatures as functions of annealing duration (t).

Figures (4.1) and (4.2) represent these results for Fe-2.02% Cu, Fe-1,56% Cu alloys respectively. It is evident in the case of both alloys that the coercive field gradually increases to its maximum value and then starts decreasing after $(H_c)_{max}$ with annealing duration.

The drop in initial permeability during annealing is much faster as compared to the increase in the coercive field. Figures (4.1) and (4.2) show that in the initial stages, while the coercive field shows hardly any change, the initial permeability has decreased to about 80% of its value within a few minutes.

It is further noted that the initial permeability increases after reaching its minimum value after longer heat treatments at higher temperature as in figure (4.1). To our knowledge this behaviour of μ_i has not been previously reported in literature.

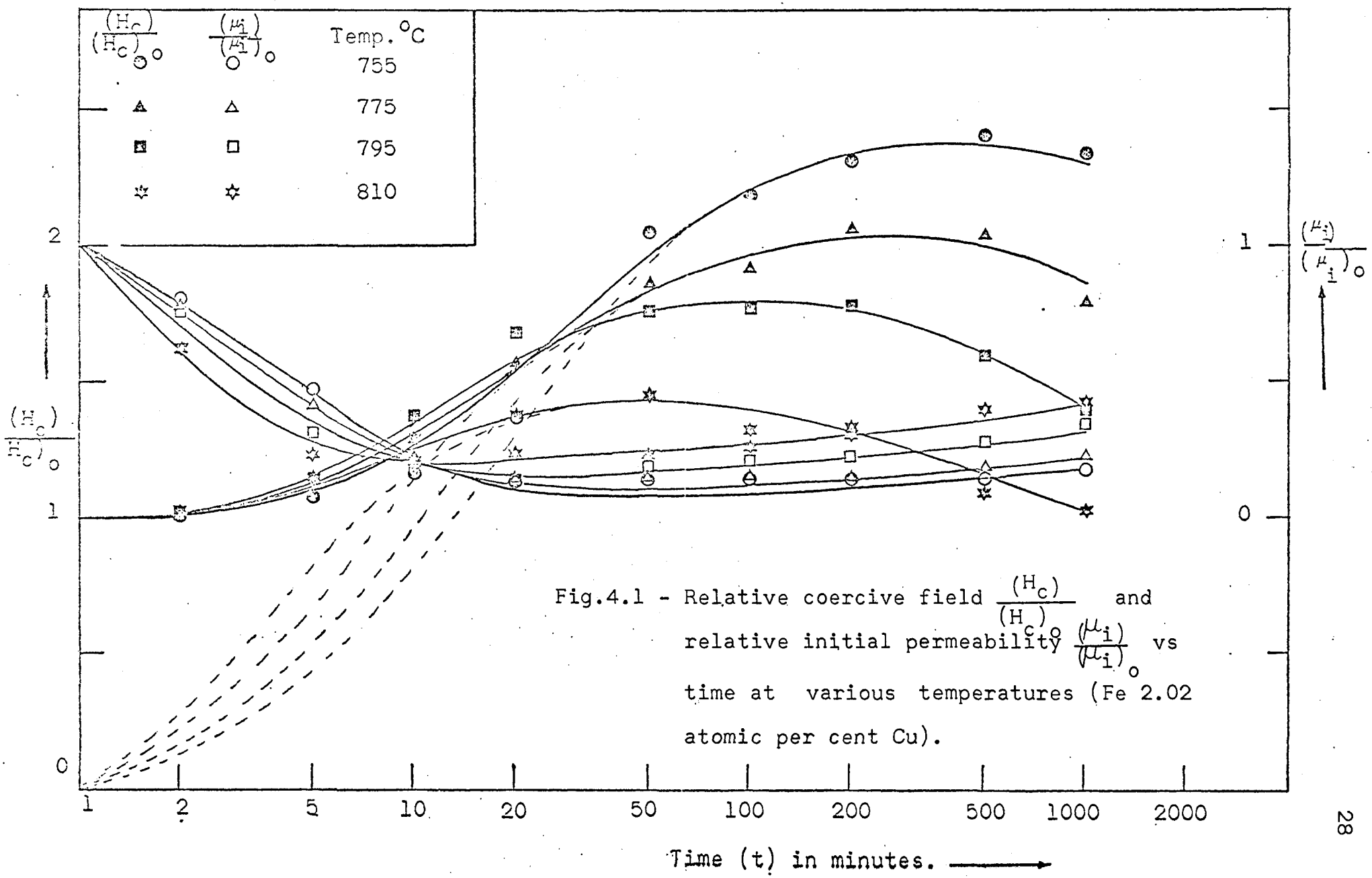

Fig.4.1 - Relative coercive field $\frac{(H_c)}{(H_c)_o}$ and relative initial permeability $\frac{(\mu_i)}{(\mu_i)_o}$ vs time at various temperatures (Fe 2.02 atomic per cent Cu).

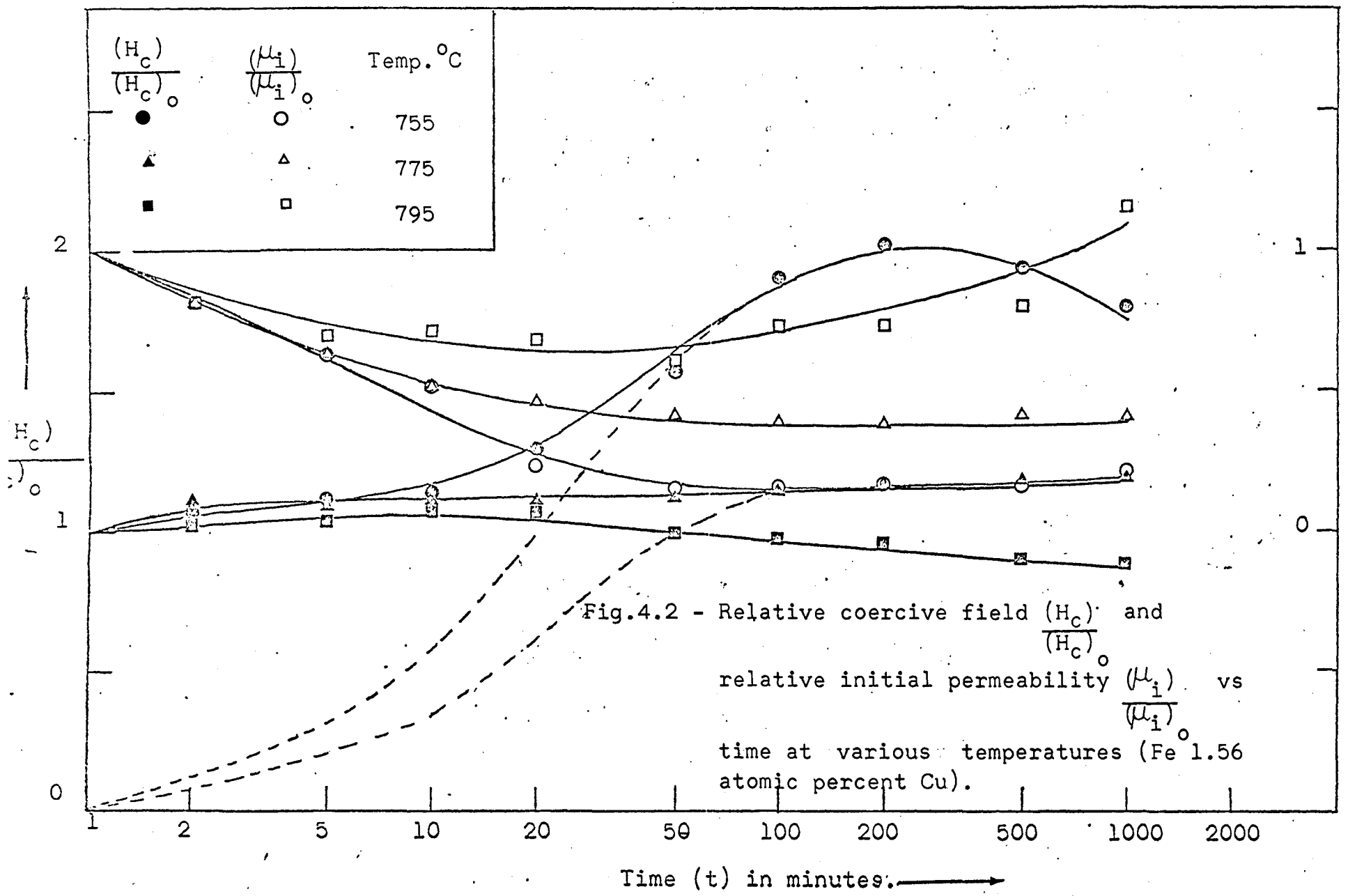

Fig.4.2 - Relative coercive field $\frac{(H_c)}{(H_c)_o}$ and relative initial permeability $\frac{(\mu_i)}{(\mu_i)_o}$ vs time at various temperatures (Fe 1.56 atomic percent Cu).

The coercive field (H_c) and initial permeability (μ_i) are both structure sensitive properties and are affected by disturbances in the matrix. In the case of the Fe-Cu alloys the predominant disturbance is the non-ferromagnetic copper precipitate in iron. The alloys in the quenched state have all the available copper in solution (maximum solubility of copper in iron is 2.14 atomic %. at 865°C.[12]) By aging the alloys at lower temperatures, the super-saturated amount of copper precipitates in fine particles, which hinder the wall movement.

The kinetics of precipitation have been explained by various authors[13][14][15][16][17]. The theoretical treatment in literature is usually based on the assumption that a fixed number of nucleation sites are available in the form of cavities, dislocations, etc. and the precipitating phase builds nuclei during the very initial stage of precipitation. These nuclei grow in size during annealing and the matrix gets gradually depleted of the precipitating phase as the process of precipitation proceeds.

We refer to the treatment of Wert and Zener[13][14][15] for the kinetics of precipitation, in which the following assumptions were made:

(1) The growth of precipitate takes place due to diffusion.

(2) The total number of precipitate particles remains constant at a certain annealing temperature.

(3) The concentration of the precipitating phase in the matrix is small.

There theoretical treatment leads to the relation:

$$\frac{\Delta C_{(t)}}{C_{(o)}} = 1\text{-}\exp.\left[-\left(\frac{t}{\tau}\right)^{n}\right] \qquad (4.1)$$

Where $\Delta C_{(t)}$ = concentration of precipitated phase after time (t)

$C_{(o)}$ = concentration of the total amount of precipitate after extremely long heat treatment ($t \to \infty$) at a given temperature.

In an attempt to interpret our results on the basis of this theory of precipitation we assume that the rise in coercive field is proportional to the amount of the precipitate in equation (4.1). We further assume that the initial value of coercive field in the Fe-Cu alloys is due to internal stresses and dislocation etc. Thus, according to equation (4.1), the coercive field is expected to follow

$$\log \ln \frac{\Delta(H_c)_{max}}{\Delta(H_c)_{max} - \Delta(H_c)_t} = n \log t - n \log \tau \qquad (4.2)$$

at all stages of precipitation.

Relation (2.4.38) has been derived with the assumption that $\Delta(H_c)_t$ is proportional to the volume of precipitated copper at various time intervals and $\Delta(H_c)_{max}$ is proportional to the precipitation of all the super-saturated copper.

Figure (4.3) shows that the slope of the lines drawn using equation (4.2) is the same in the case of both the alloys.

Wert and Zener[13],[14],[15] have interpreted the slope, (i.e. the exponent n in equation (4.1)) as an indication of the shape of the precipitate particles. In the present case with n=1, we would expect a needle-shaped precipitate.

The results in figure (4.3) have been obtained by assuming that the rise in the coercive field is proportional to the volume of copper precipitated. However, it has been reported in literature that in the case of Fe-Cu alloys with small amounts of copper, the super-saturated amount of copper precipitates completely in the very early stages of annealing[12]. In the later stages of annealing, the process of coagulation takes place and some of the particles grow at the expense of others. The annealing time required for the first stage, i.e. complete precipitation of the surplus copper, is a function of the annealing temperature and decreases as the temperature increases.

During the first stage of precipitation, the coercive field hardly changes from its original value. It is during the process of coagulation that the coercive field increases appreciably and after achieving a maximum starts to decrease slowly. This means that our assumption of the proportionality of ΔH_c to the precipitated volume of copper is not valid in this case. In spite of this discrepancy, it is interesting

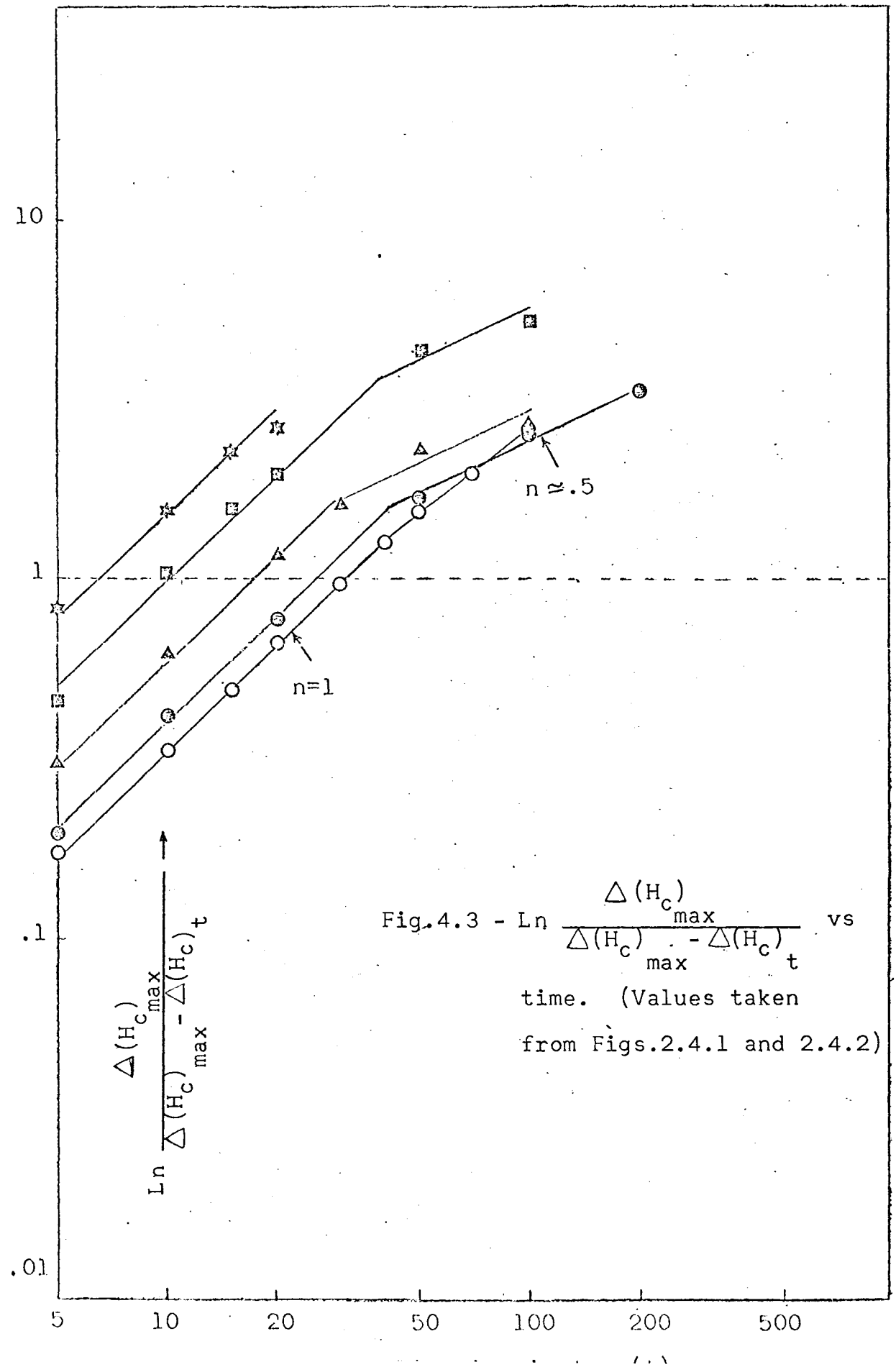

Fig. 4.3 - Ln $\frac{\Delta(H_c)_{max}}{\Delta(H_c)_{max} - \Delta(H_c)_t}$ vs time. (Values taken from Figs. 2.4.1 and 2.4.2)

to observe that the H_c results follow a similar pattern as those predicted by the theoretical consideration of Wert and Zener[13],[14][15]. This is shown by figure (4.3) when straight lines of slope n are obtained. That the coercive field is not affected by the precipitate in the early stages of annealing may be quantitatively explained in the following words: In the initial stages, the particles of the precipitate are extremely large in number and of very small size and are randomly distributed in the matrix. The Bloch wall, though tending to stick to the impurities, finds closely packed distribution of impurities everywhere inside the material and therefore can easily shift from one position to the other. It seems that the mobility of the Bloch wall is not affected to an appreciable degree before the copper inclusions achieve a critical size.

The theory put forward by Kersten[9] has the underlying assumption of a regular distribution of the precipitate particles at the corners of a cubic lattice. For the case when the size of the inclusions is smaller than the Bloch wall thickness, he derives the following relation for the maxima of the coercive field:

$$(H_c)_{max} = \text{constant} \quad v^{2/3} \qquad (4.3)$$

where v is the total volume of the precipitated phase in the matrix. Fig. (4.4) shows the maxima of the coercive field obtained in our experimental results. Also results from literature[18][19] on FeCu have been included in the

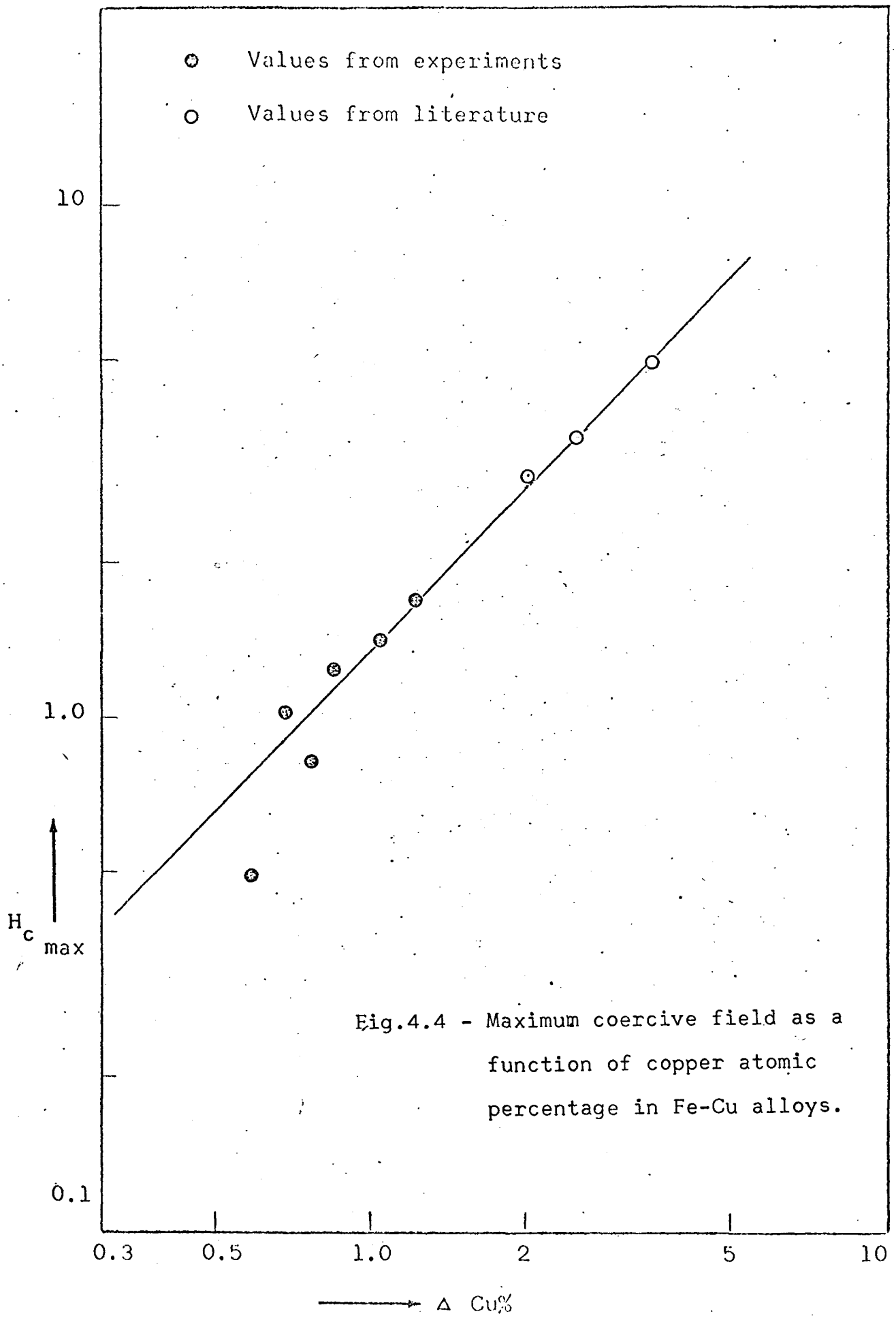

Fig.4.4 - Maximum coercive field as a function of copper atomic percentage in Fe-Cu alloys.

figure (4.4). The experimental results give a liner proportionality between $(H_c)_{max}$ and the volume of the precipitate rather than $H_{c_{max}} \text{---} v^{2/3}$ relation as proposed by Kersten.(9) The discrepancy may be due to the simplicity of Kersten's model while in fact the precipitate particles are randomly distributed. It seems that for the same volume of the precipitate the Bloch wall will include a larger number of precipitate particles if they are randomly distributed than if they lie in the simplified way on which Kersten's model is based. This causes a larger reduction in the mobility of the wall.

Kersten's theory predicts a maximum of the coercive field when the diameter of the impurity reaches the size of the Bloch wall thickness. This has also been reported by Djkstra and Wert (10) in the case of the ironcarbide precipitate in iron. Therefore, we assume that the maximum of the coercive field in our investigations also occur when the $d = \delta$. For $d > \delta$ the coercive field values drop.

The behaviour of the initial permeability μ_i is somewhat difficult to explain in the light of the present theoretical statements. It is obvious that μ_i is highly sensitive to minute traces of impurities and therefore the rapid drop in its value is obtained in the early stages of precipitation. The initial permeability is defined as the ratio between the magnetic induction B and the magnetizing

field intensity H in the Rayleigh region of the magnetization curve. We can again offer a qualititative explanation: Due to the extremely large number of the precipitate particles, the Bloch wall movement may be irreversible in the initial stages of precipitation. After long duration of aging, the number of precipitate particles decrease due to coagulation and the Bloch wall sticks to larger particles located farther apart. In such a case the magnetization in the initial stages with the application of small external fields becomes reversible again and this may also be the reason for a rise in μ_i after considerable aging.

TEMPERATURE DEPENDENCE OF THE COERCIVE FIELD:

Figure (4.5) shows the temperature dependence of coercive field. The coercive field of Fe-Cu alloys drops steadily with rising temperature up to the Curie point. The theoretical statement of Kersten [19] shows that the coercive field is a function of temperature dependent factor as K_1,

$$H_c = \text{constant} \sqrt{K_1(T)} \qquad \text{(4.4)}$$

We have drawn the theoretically expected behaviour of H_c side by side with the results obtained in our experiments and find a certain degree of agreement. The fact that the H_c in our experiments does not drop as fast as $\sqrt{K_1}$ may be due to continuous coagulation during the experiment when the measurements were taken, thus raising the value of the H_c.

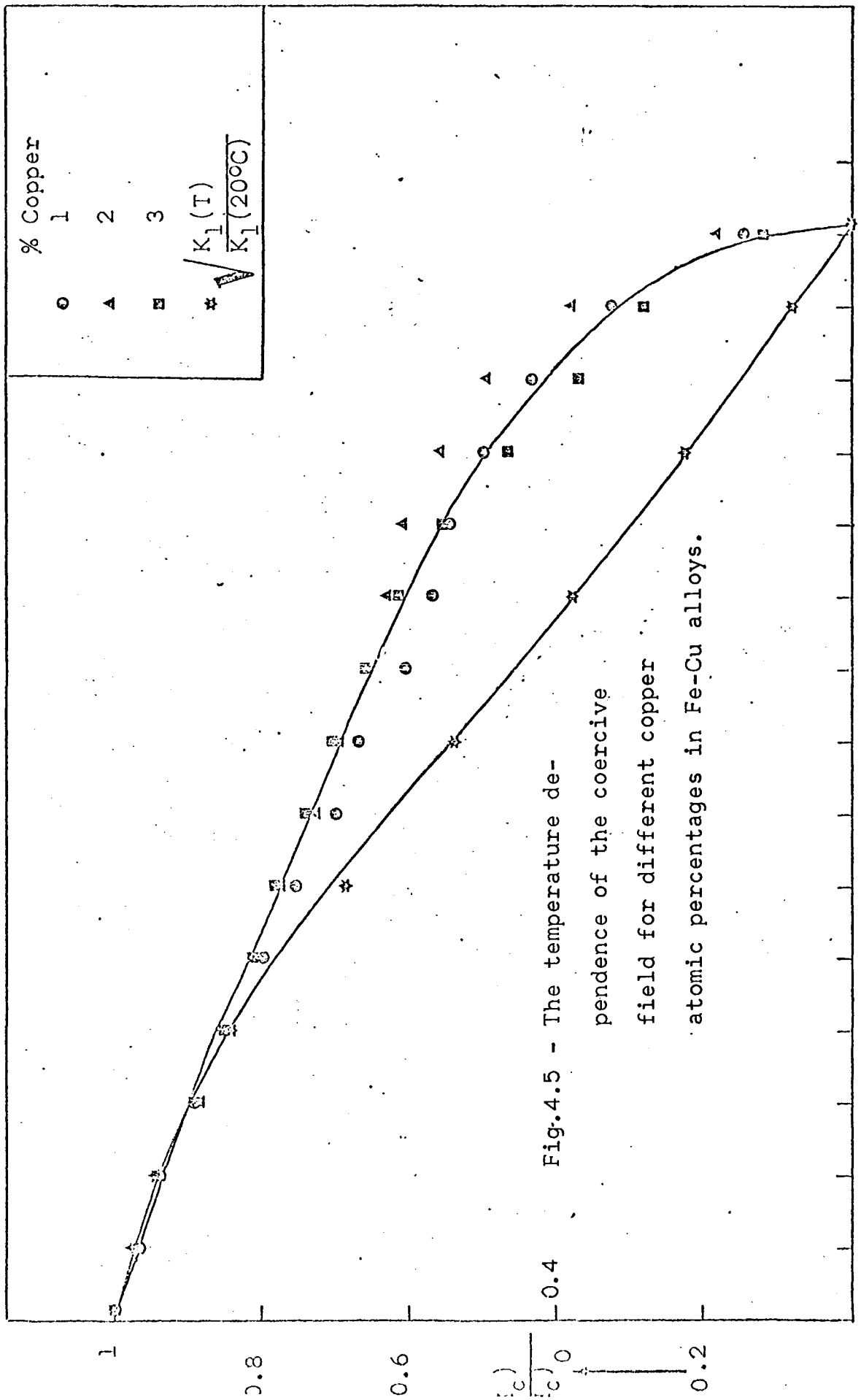

Fig.4.5 - The temperature dependence of the coercive field for different copper atomic percentages in Fe-Cu alloys.

CHAPTER V

CONCLUSIONS

1. Magnetic properties of soft ferromagnetic materials are affected adversely by the presence of non-magnetic inclusions.
2. The diffusion process is accelerated at higher temperatures which is obvious from the rapid change in the magnetic properties.
3. Technically important properties in soft ferromagnetic materials are the coercive field and the initial permeability. The effect of very small microscopic inclusions is negligible on the coercive field while the initial permeability is more sensitive to them.
4. In practical cases, one would expect a deterioration of the magnetic properties of devices using soft ferromagnetic materials having impurities initially in solution, due to aging in high temperature climates of the world. For example, carbon initially in solution may precipitate in transformer sheet steel in transformers used in high temperature climates of the world.

Appendix I

Calculations of the initial permeability and other necessary calculations:

Charge passing through the galvanometer due to magnetic flux $+\Phi$ to $-\Phi$.

$$Q = \frac{2N\Phi}{R} = K_2\,\theta$$

$$\therefore \quad \Phi = \frac{K_2 R\,\theta}{2N} \qquad \text{(i)}$$

Where K_2 = galvanometer sensitivity factor (9×10^{-3} m.coulomb/m.m.

θ = deflection (m.meter)

R = total resistance of the circuit (52 ohms)

N = number of turns in the secondary coil (4000)

Magnetic flux through the circuit if a uniform magnetic field exists along it.

$$\Phi = B\times A = \mu_0\ \mu_r\ H.A. \qquad \text{(ii)}$$

Where μ_r = relative permeability of the material

μ_0 = permeability of the vacuum ($4\pi\ 10^{-7}$ henry/meter)

A = cross-sectional area of the specimen

$\therefore$ By using (i) and (ii),

$$\mu_r = \frac{K_2 R}{2N\,\mu_0 H}\ \frac{\theta}{A}$$

$$\mu_i = 2.1\times10^{-4}\ \frac{\theta}{A}$$

Thickness of each specimen (1A, 2A, 3A and 4A) = .032 cm.

Thickness of each specimen (1B, 2B, 3B and 4B) = .022 cm.

Atomic percentage of copper in 1A, 2A, 3A, and 4A = 1.56

Atomic percentage of copper in 1B, 2B, 3B, and 4B = 2.02

TABLE 1a

Measurements of the coercive field in an isothermal heat treatment of specimens 1A and 1B at temperature 755°C for various time intervals

Time in Minutes	Sample 1A H_c(oe)		Sample 1B H_c(oe)		Sample 1A Mean Valu of H_c(oe)	Sample 1B Mean Valu of H_c(oe)
Initial Value	0.387	0.420	0.69	0.732	0.403	0.708
0	0.387	0.420	0.68	0.733		
2	0.430	0.440	0.728	0.720	0.432	0.719
	0.438	0.442	0.718	0.712		
5	0.455	0.455	0.750	0.745	0.455	0.746
	0.455	0.455	0.748	0.742		
10	0.457	0.465	0.825	0.820	0.461	0.8225
	0.457	0.465	0.825	0.820		
20	0.530	0.525	0.996	0.986	0.528	0.991
	0.532	0.525	0.998	0.986		
50	0.678	0.678	1.460	1.446	0.678	1.457
	0.678	0.678	1.464	1.458		
100	0.766	0.755	1.560	1.560	0.761	1.560
	0.763	0.762	1.560	1.560		
200	0.824	0.822	1.640	1.640	0.823	1.640
	0.824	0.822	1.640	1.640		
500	0.785	0.785	1.706	1.70	0.785	1.703
	0.785	0.785	1.700	1.706		
1000	0.726	0.732	1.670	1.650	0.728	1.659
	0.728	0.728	1.668	1.648		

TABLE 1b

Measurement of the initial permeability in an isothermal heat treatment of specimens 1A and 1B at temperature 755°C for various time intervals.

Time in Minutes	Current m.amp.	Cu 1.5% Deflection θ in mm	Cu 2% Deflection θ in mm	Cu 1.5% Initial Permeability $(\mu)_i$	Cu 2% Initial Permeability $(\mu)_i$
Initial Value 0	0.5 1.0 2.0	5.25 11.25 24.5	2.50 5.25 10.75	492	334
2	0 5 1.0 2.0	4.50 9.50 20.0	2.00 4.25 9.50	416	270
5	0.5 1.0 2.0	3.50 7.25 15.5	1.0 2.5 5.5	317	159
10	0.5 1.0 2.0	2.75 6.00 13.00	--- 1.25 2.5	262	79
20	0.5 1.0 2.0	1.25 2.75 5.5	--- .75 1.50	120	48
50	0.5 1.0 2.0	--- 1.75 3.75	--- .75 1.50	76	48
100	0.5 1.0 2.0	--- 1.75 3.75	--- .75 1.50	76	48
200	0.5 1.0 2.0	--- 2.0 4.0	---- .75 1.5	87	48
500	0.5 1.0 2.0	--- 2.0 4.0	---- .75 1.50	87	48
1000	0.5 1.0 2.0	--- 2.5 5.0	---- 1 2	109	64

TABLE 2a

Measurements of the coercive field in an isothermal heat treatment of specimens 2A and 2B at temperature 775°C for various time intervals.

Time in Minutes	Sample 2A H_c(oe)		Sample 2B H_c(oe)		Sample2A Mean Value of H_c(oe)	Sample2B Mean Value of H_c(oe)
Initial Value 0	0.398	0.385	0.700	0.695	0.391	0.698
	0.399	0.382	0.703	0.695		
2	0.445	0.420	0.710	0.695	0.434	0.699
	0.440	0.430	0.698	0.695		
5	0.430	0.420	0.732	0.745	0.427	0.737
	0.428	0.430	0.728	0.745		
10	0.445	0.435	0.845	0.832	0.434	0.833
	0.423	0.430	0.830	0.825		
20	0.450	0.425	1.110	1.094	0.435	1.102
	0.444	0.421	1.110	1.094		
50	0.452	0.426	1.310	1.292	0.441	1.301
	0.455	0.431	1.310	1.292		
100	0.455	0.441	1.354	1.326	0.447	1.340
	0.450	0.442	1.354	1.326		
200	0.462	0.462	1.450	1.460	0.464	1.446
	0.468	0.465	1.436	1.436		
500	0.485	0.495	1.430	1.390	0.490	1.406
	0.485	0.495	1.420	1.384		
1000	0.480	0.495	1.280	1.240	0.487	1.258
	0.478	0.496	1.270	1.242		

TABLE 2b

Measurement of the initial permeability in an isothermal heat treatment of specimens 2A and 2B at temperature 775°C for various time intervals.

Time in Minutes	Current m.amp.	Cu 1.5% Deflection θ in mm.	Cu 2% Deflection θ in mm.	Cu 1.5% Initial Permeability (μ_i)	Cu 2% Initial Permeability (μ_i)
Initial Value 0	0.5	9.0	3.25		
	1.0	18.25	6.75	798	429
	2.0	39.0	14.0		
2	0.5	7.25	2.5		
	1.0	15.0	5.25	656	334
	2.0	32.5	11.0		
5	0.5	5.75	1.25		
	1.0	11.75	3.0	514	190
	2.0	26.0	6.5		
10	0.5	4.5	---		
	1.0	9.5	1.5	416	95
	2.0	20	3.0		
20	0.5	4.25	---		
	1.0	8.5	1.0	372	64
	2.0	17.5	2.0		
50	0.5	3.75	---		
	1.0	7.75	1.0	339	64
	2.0	16.0	2.0		
100	0.5	3.5	---		
	1.0	7.25	1.0	317	64
	2.0	15.0	2.25		
200	0.5	6.25	---		
	1.0	6.75	1.25	295	79
	2.0	13.75	2.5		
500	0.5	3.5	---		
	1.0	7.25	1.25	317	79
	2.0	15.0	2.5		
1000	0.5	3.5	---		
	1.0	7.5	1.5	328	95
	2.0	15.5	3.0		

TABLE 3a

Measurements of the coercive field in an isothermal heat treatment of specimens 3A and 3B at temperature 795°C for various time intervals.

Time in Minutes	Sample 3A H_c(oe)		Sample 3B H_c(oe)		Sample 3A Mean Value of H_c(oe)	Sample 3B Mean Value of H_c(oe)
Initial Value 0	0.377	0.387	0.695	0.720	0.382	0.707
	0.385	0.382	0.695	0.720		
2	0.390	0.3 0	0.735	0.705	0.393	0.720
	0.390	0.405	0.720	0.720		
5	0.390	0.400	0.804	0.797	0.394	0.799
	0.391	0.397	0.800	0.797		
10	0.400	0.420	1.008	0.954	0.407	0.979
	0.391	0.420	1.010	0.944		
20	0.410	0.410	1.220	1.180	0.408	1.200
	0.400	0.415	1.210	1.190		
50	0.385	0.382	1.200	1.250	0.382	1.247
	0.376	0.387	1.260	1.250		
100	0.385	0.370	1.264	1.250	0.377	1.256
	0.380	0.375	1.270	1.240		
200	0.375	0.365	1.264	1.260	0.369	1.264
	0.375	0.362	1.274	1.260		
500	0.350	0.340	1.120	1.136	0.345	1.129
	0.350	0.340	1.130	1.130		
1000	.295	.312	1.010	0.990	0.300	1.000
	.295	.305	1.010	0.990		

TABLE 3b

Measurement of the initial permeability in an isothermal heat treatment of specimens 3A and 3B at temperature 795°C for various time intervals.

Time in Minutes	Current m. amp.	Cu 1.5% deflection θ in mm.	Cu 2% Deflection θ in mm.	Cu 1.5% Initial Permeability $(\mu)_i$	Cu 2% Initial Permeability $(\mu)_i$
Initial Value 0	0.5 1.0 2.0	7.5 15.75 33.0	3.0 6.25 13.0	689	398
2	0.5 1.0 2.0	6 12.75 27.5	2.5 5.0 11.5	558	318
5	0.5 1.0 2.0	5.25 11.0 23.5	1.0 2.0 4.5	481	127
10	0.5 1.0 2.0	5.25 11.25 24.0	--- 1.25 2.5	492	79
20	0.5 1.0 2.0	5.0 10.75 22.5	--- 1 2	470	64
50	0.5 1.0 2.0	4.5 9.75 20.5	--- 1.25 2.5	426	79
100	0.5 1.0 2.0	5.5 11.75 25.5	--- 1.25 2.5	514	79
200	0.5 1.0 2.0	5.5 11.75 24.5	--- 1.5 3.0	514	95
500	0.5 1.0 2.0	6.0 12.75 28	--- 1.75 3.5	558	113
1000	0.5 1.0 2.0	8.5 18.25 40.0	1 2.25 4.5	798	143

TABLE 4a

Measurements of the coercive field in an isothermal heat treatment of specimens 4A and 4B at temperature 810°C for various time intervals.

Time in Minutes	Sample 4A H_c(oe)		Sample 4B H_c(oe)		Sample 4A Mean Value of H_c(oe)	Sample 4B Mean Value of H_c(oe)
Initial Value 0	0.425	0.425	0.680	0.732	0.425	0.708
	0.425	0.425	0.690	0.733		
2	0.440	0.450	0.732	0.729	0.447	0.729
	0.450	0.450	0.726	0.725		
5	0.429	0.422	0.880	0.895	0.426	0.887
	0.428	0.426	0.882	0.893		
10	0.410	0.424	0.960	0.962	0.418	0.955
	0.410	0.430	0.950	0.955		
20	0.415	0.402	1.000	0.970	0.410	0.982
	0.416	0.410	0.980	0.980		
50	0.403	0.393	1.040	1.020	0.401	1.030
	0.405	0.403	1.040	1.020		
100	0.385	0.400	0.940	0.942	0.393	0.940
	0.388	0.400	0.941	0.940		
200	0.352	0.350	0.933	0.910	0.325	0.923
	0.350	0.348	0.931	0.920		
500	0.312	0.321	0.770	0.780	0.317	0.776
	0.318	0.320	0.770	0.785		
1000	0.310	0.308	0.730	0.710	0.307	0.723
	0.302	0.310	0.730	0.725		

TABLE 4b

Measurement of the initial permeability in an isothermal heat treatment of specimens 4A and 4B at temperature 810°C for various time intervals.

Time in Minutes	Current m.amp.	Cu 1.5% Deflection θ in mm.	Cu 2% Deflection θ in mm.	Cu 1.5% Initial Permeability $(\mu)_i$	Cu 2% Initial Permeability $(\mu)_i$
Initial Value 0	0.5	---	-----	525	366
	1.0	12	5.75		
	2.0	25	10.75		
2	0.5	---	---	372	207
	1.0	8.5	5.75		
	2.0	18.0	10.75		
5	0.5	---	----	372	79
	1.0	8.5	1.25		
	2.0	18.25	2.25		
10	0.5	---	----	416	64
	1.0	9.5	1		
	2.0	20.0	2.25		
20	0.5	---	----	459	79
	1.0	10.5	1.25		
	2.0	22.5	2.5		
50	0.5	----	---	470	79
	1.0	10.75	1.25		
	2.0	23.0	2.5		
100	0.5	----	----	536	95
	1.0	12.25	1.5		
	2.0	26.5	3.0		
200	0.5	---	----	536	113
	1.0	12.25	1.75		
	2.0	26.75	3.5		
500	0.5	---	---	645	127
	1.0	14.75	2.0		
	2.0	32.5	4.0		
1000	0.5	---		689	143
	1.0	15.75	2.25		
	2.0	35.5	4.75		

TABLE 5

Temperature dependence of the coercive field for Fe-Cu alloys

Temp. ^{o}C	1% Cu H_c(oe)	2.02% Cu H_c(oe)	3% Cu H_c(oe)
$^{o}7$	1.14	2.875	4.475
50	1.10	2.815	4.360
100	1.07	2.70	4.20
150	1.02	2.55	4.00
200	0.97	2.45	3.80
250	0.91	2.325	3.65
300	0.86	2.230	3.50
350	0.80	2.10	3.30
400	0.75	2.00	3.15
450	0.69	1.90	2.95
500	0.65	1.82	2.75
550	0.62	1.75	2.475
600	0.567	1.61	2.100
650	0.495	1.42	1.66
700	0.370	1.10	1.26
750	0.167	0.52	0.53
800	0.000	0.000	0.000
7^{o}	1.030	2.100	3.200

NOMENCLATURE

A	Exchange energy constant. Crossectional area of the specimen.
B	Magnetic induction (B_{rem}, remanence or residual induction).
C_o	Concentration of precipitated phase after extremely long heat treatment ($t \rightarrow \infty$) at a given temperature.
$\Delta C_{(t)}$	Concentration of precipitated phase after time(t) at a given temperature.
E_H	Energy supplied by an external magnetic field H.
E_W	Energy of the magnetic domain wall per unit area.
H	Magnetic field strength. (H_a, applied field; H_c, coercive field; H_o, critical value of H where the wall would take an irreversible displacement; H_t, total field inside the material).
$\Delta (H_c)_{max}$	Maximum increase in H_c at given annealing temperature.
$\Delta (H_c)_t$	Rise in H_c after annealing duration(t) at a given temperature.
I	Intensity of magnetization (I_s, saturation intensity of magnetization at 0^oK; I_{spon}, spontaneous magnetization).

J Quantum number. Resultant total angular momentum.

K Crystal anisotropy constant. (K_1, first crystalline anisotropy constant; K_2, galvanometer sensitivity factor).

L Orbital quantum number. ($\vec{L}$, resultant orbital vector).

M Magnetic moment. (M_B, Bohr magneton).

N Molecular field constant. Number of turns in the secondary coil of the permeability measurement core.

P Angular momentum. Pressure exerted on the magnetic domain wall.

Q Charge through galvanometer.

S Total area of the magnetic domain wall. Spin quantum number ($\vec{S}$, resultant spin vector).

T Temperature(Kelvin);(T^{o}_{C}, temperature centigrade).

W Work done by the magnetic field.

d Diameter of precipitate.

e Charge of an electron.

g Gyromagnetic ratio.

h Planck constant.

k Boltzmann constant.

ℓ Wave length of the spatial variation of internal stress. Lattice constant.

m Mass of an electron.

n	An integer. Constant which determines the shape of the precipitate.
r	Radius of curvature of the magnetic domain wall. (r_e, radius of an electronic orbit).
v	Total volume of the precipitated phase.
Δv	Change in the volume of a magnetic domain.
x	Displacement along x axis.
α	Curvature of potential valley inside the material.
γ	Surface energy of the magnetic domain wall.
δ	Bloch wall thickness.
θ	Deflection.
λ	Magnetostriction constant. (λ_{100}, Magnetostriction constant for the direction $\left[100\right]$,λ_{111}, magnetostriction constant for the direction $\left[111\right]$).
μ_i	Initial permeability. (μ_o, permeability of vacuum; μ_r, relative permeability of the material).
Θ	Curie temperature.
σ	Stress inside the material.
τ	Time constant depending on C_o.
Φ	Angle between direction of H and direction of I_s. Magnetic flux.
χ	Volume susceptibility.
ω	Angular velocity of an electron.

BIBLIOGRAPHY

1. Physics of Magnetism by Soshin Chinkazumi, John Wiley & Sons,Inc., New York

2. Ferromagnetism by Richard M. Bozortti, D.VanNostrand Co.,Inc., Princeton, N.J.

3. The Solid State for Engineers by Maurice J. Sinnott, John Wiley & Sons,Inc., New York

4. Magnetism in Solid by D.H. Martin, The M.I.T. Press, Massachusetts Institute of Technology, Cambridge, Mass.

5. E. Konsorsky: Physik.Z.Sowjetunion, 11,597(1937)

6. M. Kersten: Physik Z 39,860(1938)

7. L. Neel: Ann.Univ. Grenoble 22,299(1946)

8. M. Kersten: Z.Angew.Phys.7,313(1956);8,382,496(1956)

9. M. Kersten: Probleme der technischen Magnetisierungskurve, edited by Becker (Verlag Julius Springer, Berlin; reprinted by J.W. Edwards, Ann Arbor, 1938), pp 42-72; G.3,p.215

10. L.J. Djikstra and Wert, Phys.Rev. 79(1950) 979

11. A.H. Qureshi: Conference on Magnetic Materials and their Application, Conference Pub.33,Sep.1967

12. A.H. Qureshi: Z.f.Mellalkunde, 52(1961) 799

13. C. Wert: J.Applied Physics; 20(1949) 943

14. C. Zener: J.Applied Physics; 20(1949) 950

15. C. Wert and C.Zener; J.Appl.Phys. 21(1950) 5

16. Precipitation from Iron-base alloys, Metallurgical Society, Volume 28(1963) (1-66)

17. The Theory of Transformation Metals and Alloys, by J.W. Christian(1965) Pergamon Press, Chap. XVI.

18. A. Kubman und B. Scharnow, Z.Physik 54(1929),S.1;vgl.auch. A. Kubman, Arch. Elektratechn (29)(1935), S.297

19. H. Buchholtz und W. Koster, Stahl und Eisen 50(1930),S.690

20. M. Kersten; Zeitschrift fur angewandte Physik,8.Band,10, Heft,1956, S.496-502.

VITA AUCTORIS

1942 - Born October 3rd 1942 in District Bannu, Pakistan

1958 - Received Matriculation Certificate from Government High School no.2, Bannu, Pakistan

1963 - Received B.Sc.(Hons) Physics Degree from University of Peshawar, Pakistan

1964 - Received M.Sc. Physics Degree from University of Peshawar, Pakistan, and the University Gold Medal for standing first among all the candidates

1964-67 - Worked as a Lecturer of Applied Physics in the Faculty of Engineering at the University of Peshawar, Pakistan

1967-70 - Studied for Master of Applied Science Degree at the University of Windsor, Canada.